Journal of Hydrology: Regional Studies 46 (2023) 101352

Contents lists available at ScienceDirect

Journal of Hydrology: Regional Studies

journal homepage: www.elsevier.com/locate/ejrh

Deciphering Hulun lake level dynamics and periodical response to climate change during 1961–2020

Yuqi Huang [a,b,c], Bo Yao [d], Yu Li [a,b,c], Hao Zhang [a,b,c], Shengrui Wang [a,b,c,*]

[a] College of Water Sciences, Beijing Normal University, Beijing 100875, China
[b] Guangdong-Hong Kong Joint Laboratory for Water Security, Center for Water Research, Advanced Institute of Natural Sciences, Beijing Normal University at Zhuhai, 519087, China
[c] Engineering Research Center of Ministry of Education on Groundwater Pollution Control and Remediation, College of Water Sciences, Beijing Normal University, Beijing, 100875, China
[d] Key Laboratory for Mechanics in Fluid Solid Coupling Systems, Institute of Mechanics, Chinese Academy of Sciences, Beijing, 100190, China

ARTICLE INFO

Keywords:
Lake
Water resources
Climate change
SEM
Landuse

ABSTRACT

Study Region: Hulun Lake, the fifth largest lake in China.
Study Focus: The notable decline in water level (WL) caused by climate change is the primary challenge faced by Hulun Lake. However, the contribution of climate to water loss and its driving mechanisms remain unclear. The impact of climate on WL change was investigated using wavelet analysis and structural equation models.
New Hydrological Insights for the Region: In the past 60 years, the increasing potential evapotranspiration (ET_p) caused by warming climate was the main reason for the WL decline (r=−0.67). For period I (1961–1997), reduced runoff due to increasing ET_p caused an overall decrease in WL (r = 0.41). During the mid-1980s, the increase in rainfall driven by ENSO (r = −0.66) caused a slight increase in WL (r = 0.31). For period II (1998–2020), deforestation, farmland and urban area expansion were the main drivers behind the significant increase of ET_p in the watershed (r = −0.22), which leads to reduced runoff and, consequently, a significant decrease in WL. The influence of climate on WL change weakened compared with that in the first period due to land use change (r = −1.08).

1. Introduction

Lakes respond rapidly to climate change, especially in arid and semi-arid regions (Woolway et al., 2020; Woolway and Merchant, 2019). Some manifested consequences include decline in water volumes, increased water temperature, ecosystem degradation, etc (Yang et al., 2019, 2020). As a sentinel to climate change, water level (WL) regime is also an intuitive indicator of lake water resources (Kraemer et al., 2020), which can comprehensively reflect hydrological processes (e.g., runoff generation, evapotranspiration and rainfall) of the basin and the abundance of lake water storage. In the past decades, global warming and anthropogenic activities have caused a sharp decrease in WL in closed inland lakes in northern China. The number of lakes larger than 1 km^2 in Inner Mongolia decreased by 159 between 1991 and 2009 (Zhou et al., 2019). There is an impending need to investigate the impact of climate change on lake WLs in semi-arid and arid regions for watershed management and lake water conservation.

Among all drivers, climate change has shown a widespread impact on lake WLs in arid regions. Due to the complexity and nonlinearity of climate factors, their impact on WL typically manifests across different time spans (Rezaei and Gurdak, 2020). With

* Corresponding author.
E-mail address: wangsr@bnu.edu.cn (S. Wang).

https://doi.org/10.1016/j.ejrh.2023.101352
Received 27 November 2022; Received in revised form 19 February 2023; Accepted 22 February 2023
Available online 9 March 2023

the gradual strengthening of human activities, the dual influences on the evolution of watershed environment and on WL requires a more thorough and discreet verification (Cooley et al., 2021). Climate impact on lake WL has drawn great attention in recent years, where researchers applied different approaches to reveal the response and driving mechanism of lake WLs against various changing climatic factors. Those methods include statistical models (such as the least squares regression model and Bayesian network), conceptual models (such as the Budyko hypothesis and SCS-CN models) (Wang, 2018; Zhang et al., 2015) and process-based models (such as SWAT, Delft3D) (Chen et al., 2018; McCombs et al., 2014). These methods tend to focus on the impact of individual variables (e.g., precipitation, air temperature and runoff) on WL. However, lake WL variation often results from complex interactions between meteorological factors, such as evaporation and precipitation, as well as from watershed hydrological factors such as inflow (Kundu et al., 2017). How to disentangle such interaction in the context of changing conditions remains a challenge. By considering the interaction between independent variables, SEM can effectively quantify the combined effect of multiple influencing factors on target variables (Jia et al., 2020; Song et al., 2021). It can be used to distinguish the direct and indirect effects of hydrometeorological factors on WL change and is thus considered a powerful method for better WL attribution analysis.

Hulun Lake is the largest lake in northern China and plays a substantial role in water conservation, biodiversity maintenance, and climate regulation (Cao et al., 2021a). Since it is located in the middle and high latitudes of the marginal area affected by the southeast monsoon, the regional hydrological cycle is relatively sensitive to climate change. In recent decades, the WL of Hulun Lake has shown a significant downward trend (Liu and Yue, 2017), with prominent ecological and environmental problems such as wetland shrinking and water quality deterioration (Fang et al., 2019). Although many studies have applied machine learning algorithms, water balance models and other approaches to analyze the attribution of WL decline under climate change (Cai et al., 2016; Fan et al., 2021), few of them considered the interactions of multiple factors when explaining the driving mechanism. In addition, with increasing droughts in the basin, the intensification of human activities and significant land use changes in recent years (Zhang et al., 2019), it still remains unclear how the contribution of climate to WL changes over time, and the underlying driving mechanism requires further clarification to improve the management strategy of Hulun Lake WL.

This study aims to explore the influence of climate on WL change in Hulun Lake from 1961 to 2020. Based on wavelet analysis and the SEM, the purpose of this study is to: (1) analyze the characteristics of regional climate and lake level change; (2) quantify the contribution of climate change to WL variation; and (3) explore the driving mechanism of WL changes in Hulun Lake during different periods. The results can provide a scientific basis for the management of Hulun Lake and water resource protection in the basin and also provide important information for revealing the driving mechanisms of lake WL changes in other cold and arid regions under changing climate.

2. Data and methodology

2.1. Study area

Hulun Lake (48.30°–49.20°N, 117°–117.41°E) is located in the western part of the Hulun Buir grassland in Inner Mongolia (Wu et al., 2015), close to the borders of China, Mongolia and Russia (Fig. 1). The lake area is approximately 2134.05 km^2 with an average depth of 4.71 m. The lake basin features a typical temperate continental climate, with 90% of the area covered by grasslands (Xiao et al., 2009). Rainfall is concentrated in summer, accounting for about 72.2% of the annual total amount, and the average temperature is around −1.36 °C. Winter lasts from mid-October to early May, which is also the glacial period of the lake.

There are over 60 rivers and streams in the basin, of which Kherlen and Urshen are the largest. The Kherlen River, located southwest of Hulun Lake, originates from the eastern foot of the Khentii Mountains in the People's Republic of Mongolia. It flows from west to east before entering Hulun Lake, with an average annual runoff of 4.6×10^8 m^3. The Urshen River originates from the Greater Khingan Mountains southeast to Hulun Lake, with an average annual runoff of 6.11×10^8 m^3. Runoff, precipitation and evapotranspiration are the main components of the multi-year water balance of Hulun Lake (Fu et al., 2021).

Since 2000, Hulun Lake did not discharge any outflow due to the WL decline. To remediate the situation, in 2010, the local government excavated an artificial channel in the northeast of the lake to divert Hailar river into Hulun Lake during flood season (Li et al., 2021).

2.2. Datasets

Monthly WL data of 1992–2020 was obtained from Hydroweb (http://hydroweb.theia-land.fr) developed by the Laboratoire d'Études en Gèo-physique et Océanographie Spatiales (LEGOS), which has been proven a reliable dataset by multiple scholars (e.g. Cretaux et al., 2011; Liu and Yue, 2017). [Annual] in-situ WL observations for 1961 to 2011 were obtained from the Dalai gauge (49°08', 117°22'). The overlapping period (1992–2011) between the LEGOS altimetry and the in-situ measurements showed a high correlation (r^2 = 0.99; see Fig.S1). Then, the two datasets were merged together to construct a long time series (1961–2020) to be used in this study. The meteorological data were obtained from Climatic Research Unit (CRU), which provides interpolated grid datasets for 4000 gauging stations worldwide across a long time scale (Harris et al., 2020). In this study, four climate variables, namely precipitation (Pre), potential evapotranspiration (ET_p), surface temperature (Tmp), and vapor pressure (Vap), were downloaded from CRU TS Version 4.05 product (https://crudata.uea.ac.uk/cru/data/hrg/cru_ts_4.05/) for 1961 to 2020. Sea surface temperature (SST) anomalies in the Niño 3.4 regions were obtained from NOAA (https://www.esrl.noaa.gov/psd/gcos_wgsp/Timeseries/Nino34/) to represent ENSO [(El Niño-Southern Oscillation)] intensity. Using SST data, we calculated the ENSO index for December to February and the NAO (North Atlantic oscillation) index for November to March. Landcover data from 1992 to

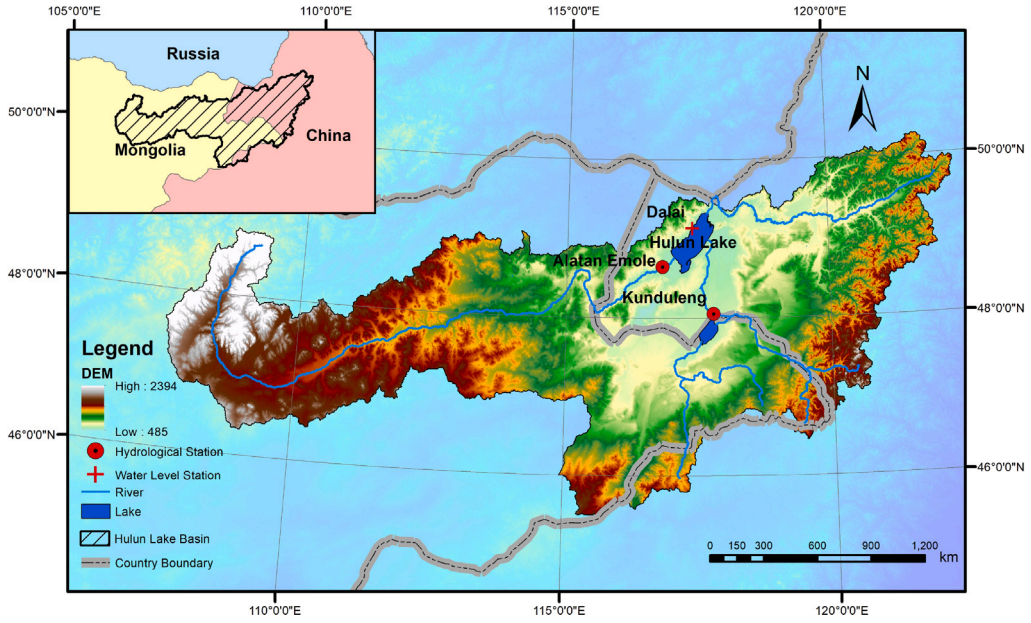

Fig. 1. The geographical location of Hulun Lake and its watershed.

2020 were obtained from the European Space Agency Climate Change Initiative. The dataset has a spatial resolution of 300 × 300 m and includes 37 landuse types (Hollmann et al., 2013), which were then reclassified into 8 categories (i.e., cropland land, forest, grassland, bare land, vegetation, water body, urban land, and others). The standardized precipitation evapotranspiration index (SPEI), downloaded from the institutional repository of the Spanish National Research Council (http://digital.csic.es/), was used to indicate the droughts in the watershed.

2.3. Methods

2.3.1. Abrupt change point detection

The Mann–Kendall (M–K) significance test and moving t-test were performed to identify abrupt change points of WL variation during 1961–2020. The M–K test is a non-parametric statistical test that is widely used to evaluate the trends of hydrological time series (Guclu, 2018). A positive value of the forward curve (UF) indicates an increasing trend of a time series, while a negative value indicates a decreasing trend. The intersection of the UF and backward curve (UB) within 5% confidence interval is identified as a change point. The moving t-test can detect whether the mean values of the two sub-samples change significantly (Zhao et al., 2015). Both methods are widely applied in the field of hydrology. The M–K test and moving t-test were implemented in MATLAB R2020b.

2.3.2. Wavelet analysis

The wavelet analysis can reveal the local characteristics of a time series in time–frequency domain, making it suitable for studying hydrometeorological time series with multiple time-scales and nonstationary characteristics (Labat, 2005; Labat et al., 2005). A wavelet is a wave-like oscillation with an amplitude that begins at zero, increases or decreases, and then returns to zero. The wavelet function should satisfy the following conditions:

$$\int_{-\infty}^{\infty} \psi(t)dt = 0 \tag{1}$$

Where $\psi(t)$ is the basic wavelet function. The continuous wavelet transformation of signal $f(t) \in L^2(R)$ can be expressed as:

$$\begin{aligned} W_f(a,b) &= \int_{-\infty}^{\infty} f(t)\psi^*_{a,b}(t)dt \\ \psi_{a,b}(t) &= \frac{1}{\sqrt{a}}\psi\left(\frac{t-b}{a}\right), a, b \in R, a \neq 0 \end{aligned} \tag{2}$$

$W_f(a,b)$ is the wavelet transform coefficient; $\psi^*(t)$ is the complex conjugate function of $\psi(t)$; a is the scale factor that reflects the period length of the wavelet and b is the shift factor, which is the shift in reaction time.

Wavelet coherence (WTC) was applied to identify the frequency bands within which two time series co-varied and can be defined as:

$$R_n^2(a) = \frac{|b^{-1}W_f^{XY}(a)|^2}{S(a^{-1}|W_f^X(a)|^2) \cdot S(a^{-1}|W_f^Y(a)|^2)} \tag{3}$$

Where $R_n^2(a)$ presents wavelet coherence, and S is a smoothing operator for both scale and time domain which is defined as:

$$S(W) = S_{scale}(S_{time}(W_n^S(s))) \tag{4}$$

Where S_{scale} smooths along the scale axis and S_{time} smooths along the time axis. The wavelet coherence spectrum quantitatively measures the cross-correlation of two factors in multiple temporal scales.

2.3.3. WL influence factor quantifications

Two coherence indicators, namely single-scale coherence rate (SCR) and percentage area significant coherence (PASC), are defined to assess the influence of individual factors on WL at different scales and to quantify the coherence relationship between WL and climate factors.

$$\begin{aligned} \mathrm{SCR}_c &= \frac{N_{cs}}{N_{ts}} \\ \mathrm{PASC}_c &= \frac{A_s}{A_t} \times 100\% \end{aligned} \tag{5}$$

where N_{cs} represents the number of years in which the WL coherence index is larger than 0.5 at scale s; N_{ts} refers to the total number of years at scale s, which equals 60 in this case. SCR_c was used to quantify the coherence relationship between WL and the climate factor (c) at the scale s. The higher the SCR_c, the more years the influencing factor f is significantly coherent with WL at scale s. For climate factor c, a high value of SCR_c also indicates strong multi-scale stability of coherence relationship between WL and climate factor c. A_s is the area of significant coherence patches; A_t is the total area of coherence, which is the same for all climate factors; PASC_c reflects the significant extent of coherence between climate factor c and WL across all years and scales. The larger the value of PASC_c, the more significant coherence between climate factor c and WL.

2.3.4. Structure equation model (SEM)

SEM has now been widely used in different disciplines (Grace et al., 2014; Hao et al., 2020; Yang et al., 2021). Compared with other models, SEM can effectively quantify the combined effects of multiple influencing factors on target variables by considering the interactions between independent variables. In a complete SEM analysis, a set of hypotheses between several variables based on the results of theoretical basis or prior research should first be constructed. The fitting indicators must then be modified until they meet statistical requirements (Henseler et al., 2015). Typically, SEM includes observed and latent variables. The observed variables can be directly measured and are represented by squares or rectangles. Latent variables are used to describe unobserved variables that can be explained by observed variables and are expressed as circles or ellipses.

SEM adopts a maximum likelihood estimation using goodness-of-fit indicators, such as the comparative fit index, root mean square error of approximation, and standardized root mean square residual. The standardized regression coefficient (r) represents the influence of two factors, where a positive value indicates a positive influence. In this study, we considered flow, ENSO, NAO and four climate factors as the observed variables, while land use change as the latent variable.

3. Results

3.1. Characteristics of WL variation

The WL of Hulun Lake fluctuated significantly over the past 60 years, with an average level of 543.9 m and a decreasing trend of 0.41 m/a (see Fig. 2a). As shown in Fig. 2b–d, the intersection of the positive and inverse sequence lines of the M–K test is in 1972, 1990, and 1997, whereas only 1997 is within the 5% significance level. Among positive peaks of the t-test curves for the 5-year and 15-year sliding windows, the 1997's peak exceeded the confidence interval. Therefore, 1997 was one abrupt change point of WL. Based on abrupt point detection, changes of the WL can be divided into two periods: a slow declining period (1961–1997) and a drastic fluctuating period (1998–2020). In the first period (1961–1997), the WL decreased slightly by 7 mm/a. During 1961–1983, the WL dropped by 1.8 m from 544.9 m to 543.1 m, after which WL experienced successive increases in years 1984, 1985, and 1986, rising from 543.8 m to 545 m, and then fluctuated at approximately 544.8 m. In the second period (1998–2020), the WL declined dramatically, with an overall declining rate of 37.6 mm/a. During 1998–2011, the WL dropped sharply by 3.47 m, from 544.52 m to 540.97 m at a rate of 330 mm/a. Then, WL experienced a recovery period after 2012, rising from 540.96 m to 543.84 m in 2020, which is consistent with the observed records by Jason satellite data (Li et al., 2019).

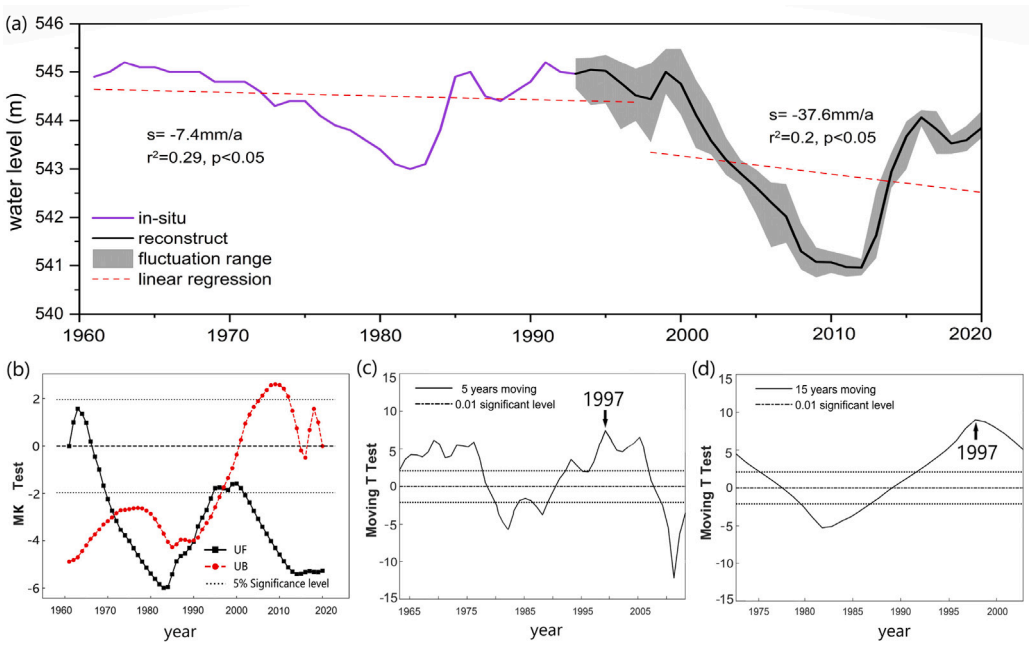

Fig. 2. The inter-annual variation of the Hulun Lake WL from 1961 to 2020 (a), and the abrupt changing point identification diagram of Hulun Lake WL, where (b) is the positive and negative sequence line of the Mann–Kendall (MK) test; (c) is the sliding t-test curve with a moving window of five time-steps and (d) fifteen time-steps, respectively.

3.2. Variation of hydrometeorological factors

Climate change is known as an important driver in altering hydrological processes. In this study, ET_p, Pre, Tmp and Vap were selected to investigate the impact of climate change on Hulun Basin over the past 60 years. Fig. 3a–d depict the temporal trends of meteorological factors in Hulun Basin. Results show that, although the annual Pre in the Basin barely shows an upward trend (0.1 mm/a), a transition from dry to wet years is evident during 1978–2000, and the turning point occurred approximately in 1986. Meanwhile, the WL rose from 543.8 m to 545 m during 1984–1986. Therefore, the change of Pre is well correlated with the WL variation during this period. Vap also showed an upward trend (0.7 hpa/10 a). A climate transition from wet to dry during mid-1990s was detected from the LOWESS curve, and the turning point was approximately in 1997. Subsequently, Vap decreased at a rate of 0.16 hpa/10 a. The decrease of Vap might be explained by the slight decrease in summer Pre during this period (Fig.S2a), causing less water to evaporate into the atmosphere (Li et al., 2022). As shown in Fig. 3d, during 1961–1997, the ET_p is relatively stable, with an increasing trend of 0.16 mm/a; After 1997, however, the annual ET_p increased significantly at a rate of 0.9 mm/a, with the annual and monthly averages significantly improved during this period (see Fig.S2b). Tmp in Hulun Basin showed a significant upward trend (0.3 °C/10a) and increased by approximately 1.8 °C in the past 60 years. In addition, an upward trend occurred in both ice-covered and none ice-covered periods (Fig.S2c), with rates of 0.31 °C and 0.32 °C/10a, respectively. Overall, Hulun Basin is undergoing a warming and drying transition over the past 60 years, with an intensified trend in the 21st century due to the increase of ET_p.

The pattern of the wavelet coefficient of Vap is similar to that of Pre, while the pattern of ET_p is roughly the opposite of Pre and Vap, indicating strong correlations among the three variables. There are two high-value centers on 45- and 55-year scales for strong ET_p years (1975 and 2010), and one low-value center for weak ET_p year (1992). Tmp showed multiscale characteristics, with multiple warm and cold centers. Overall, the patterns among Pre, Vap, and ET_p were consistent with the WL variation.

3.3. Relationships between water level and climatic variables

To better understand the impact of climate change on WL variation, the correlation between each climate factor and WL was analyzed. As shown in Table 1, the correlation coefficients between WL and ET_p reached −0.57, followed by Pre, with r being −0.37. The correlations between WL, Tmp, and Vap were relatively low and none-significant ($p>0.1$). Overall, ET_p was significantly correlated with WL changes.

To further investigate the influence of climate factors on the WL at different time scales, WTC was calculated to quantify the linearity between WL and climate factors in time–frequency domain. According to the results, WL showed a high response to ET_p and Tmp, followed by Vap and Pre. During 1966–1974 and 1984–1994, WL showed a lag of six-month behind concurrent precipitation (see Fig. 4e). Similar to Pre, WL lagged behind Vap by six months during 1961–1985 (Fig. 4g), while WL showed in-phase correlations

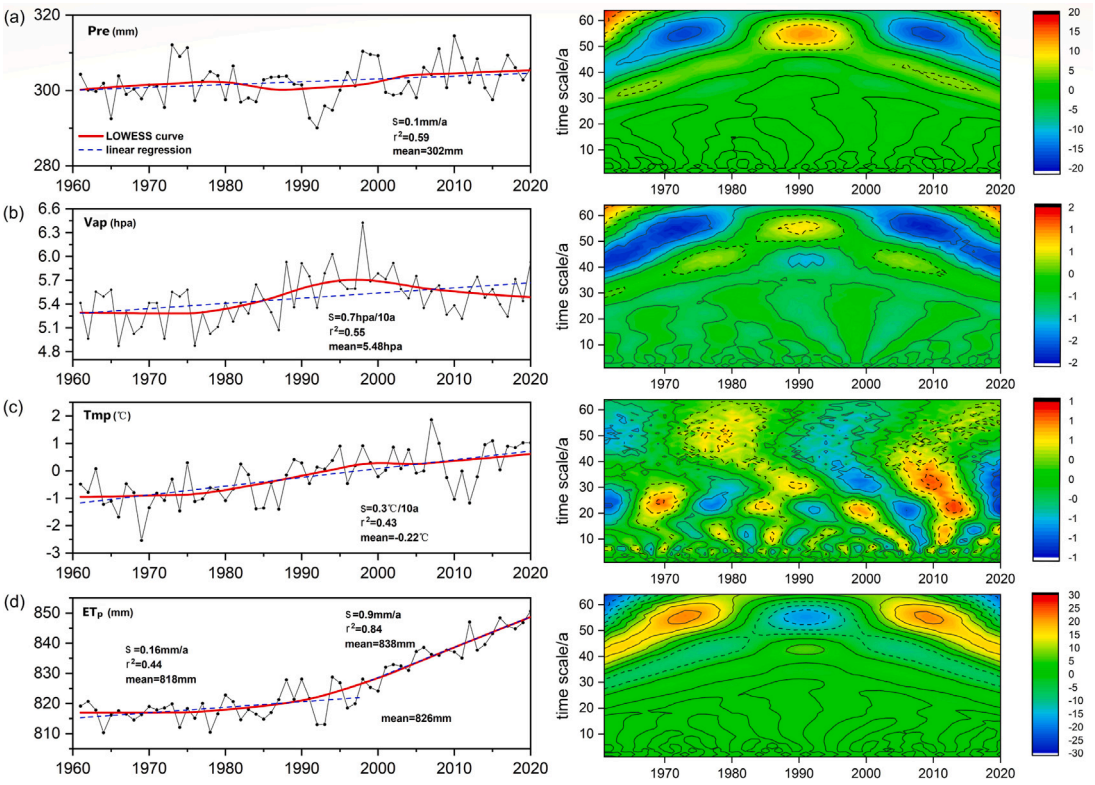

Fig. 3. Annual average of (a) precipitation, (b) vapor pressure, (c) temperature, and (d) potential evapotranspiration in the basin during 1961–2020. The red line shows the time series smoothed using LOWESS filtering. Dotted line represents linear regression of time series. The right panel illustrates the isoline of the real part of Morlet wavelet coefficients, which reflects the periodic changes of the variables at different time scales and their distributions in time. (For interpretation of the references to color in this figure legend, the reader is referred to the web version of this article.)

Table 1
Results of correlation analysis between the WL and climatic factors in Hulun Lake Basin.

	ET_p		Pre		Tmp		Vap	
	r	*p*	*r*	*p*	*r*	*p*	*r*	*p*
Spearman	−0.57	<0.01	−0.37	<0.01	−0.33	0.07	0.03	0.836

with Vap around 2000. During this period, the basin showed an overall drying trend. Vap decreased gradually, as did WL. The WTC characteristic of Tmp was similar to that of ET_p, where, during 1970–1990, WL showed a significant negative correlation with Tmp and ET_p (Fig. 4f and h), indicating a decrease of WL with respect to the increasing Tmp and ET_p. Notably, the synchronization relationship among Tmp, ET_p, and WL changed during 2004–2020 and 1990–2010. Specifically, the WL series was ahead of Tmp and ET_p by approximately 45°. However, the increase in Tmp during 2004–2020 could not explain the variation in WL. In addition, the positive correlation between ET_p and WL from 1990 to 2010 is inconsistent with the observed increase of ET_p. Thus, one might infer that factors other than climate change (such as human activities) may have played a leading role in the drastic change of WL in Hulun Lake in the late 1990s.

The cumulative SCR of climate factors was calculated to quantify the coherence relationship between each climate factor and WL at different scales. According to the results shown in Fig. 5a, the SCR of Pre and Vap were mainly concentrated on medium and small time scales: SCR_p was concentrated within 9 years, while SCR_v within 6 years. SCR_e was mainly concentrated on medium-and long-term scales (greater than 6 years), while SCR_t spanned across all years, indicating multiple time-scale impacts on WL. Notably, all climate factors have significant coherence with WL within a 4-year scale, which is a typical scale of ENSO (2–7 years). On the scales of 11- to 12-year that are typical for the NAO (11 years), the SCR of each climate factor reaches the maximum. The SCR results highlighted the potential relationship between atmospheric circulation and climate change in Hulun Basin.

Fig. 5b shows the contribution of each climate factor to the WL variation at different periods. ET_p contributed the most in the past 60 years, where $PASC_e$ = 9.6%, followed by Tmp ($PASC_t$ = 8.8%). Vap and Pre have less influence on WL, with PASC=5.9% and 2.7%, respectively. The PASC of Pre and Vap were larger during the first period, indicating that the impacts of the two variables on WL were mainly concentrated during 1961–1997. Instead, the PASC values of ET_p and Tmp for the two periods were similar, implying that ET_p and Tmp contribute almost the same in both periods to WL variation. It is worth noting that the average PASC of

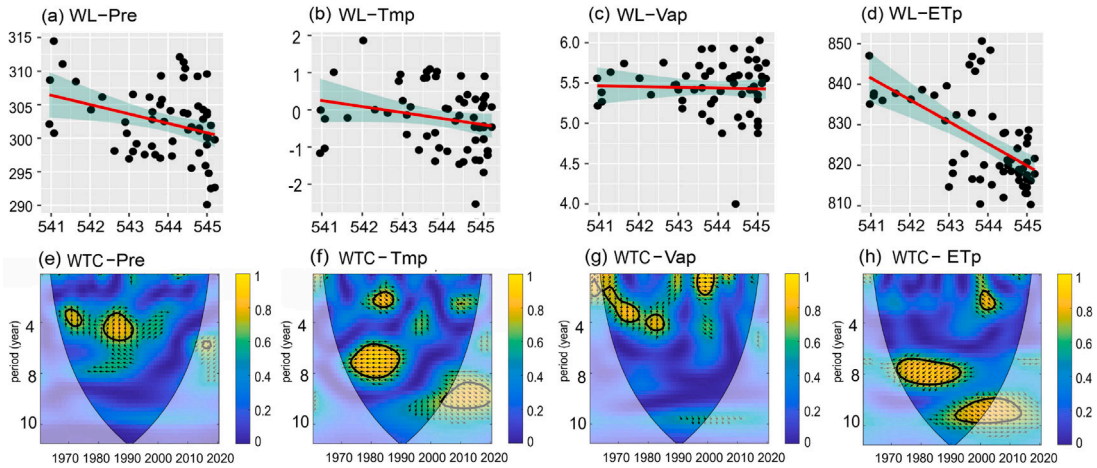

Fig. 4. Correlations between Hulun Lake WL and (a) Pre, (b) Tmp, (c) Vap, and (d) ET_p. The straight lines are linear regression lines, with the shades being the 95% confidence bands. The lower panel shows the wavelet coherence (WTC) between WL and (e) Pre, (f) Tmp, (g) Vap, and (h) ET_p. The color bar states the spectral power, and the thick black contour indicates the 95% confidence level, and the less intense colors specify the cone of influence. Black arrows are the phase angle, indicating the phase relation between two series for which right- and left-pointing arrows refer to in-phase and anti-phase relations, respectively. Furthermore, upward (downward) arrows are indicative of lead (lag) between the time series. (For interpretation of the references to color in this figure legend, the reader is referred to the web version of this article.)

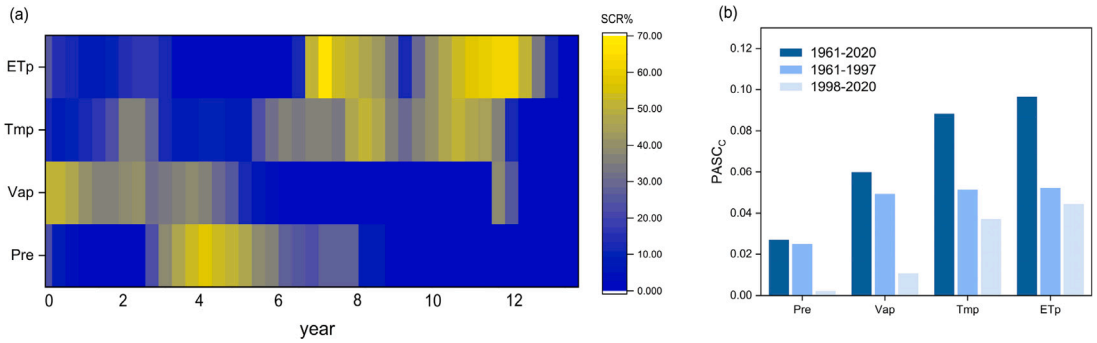

Fig. 5. (a) SCR_c for all WL influencing factors at each scale. (b) $PASC_c$ for each influencing factor on WL during the entire period, the first and second periods, respectively.

all climate factors during 1961–1997 (denoted as PASCI) was greater than that during 1998–2020 (PASCI=4.43% > PASCII=2.34%), which infers a weakening impact of changing climate on WL variation towards late 20th century.

According to the results, WL variation highly correlates with ET_p, followed by Tmp. The impact of Vap and Pre on WL weakened after the end of the 20th century, except for ET_p and Tmp.

4. Discussions

4.1. Underlying mechanisms of water level variation in different periods

Hulun Lake is located at the junction of the monsoon and non-monsoon regions, and its hydrological cycle is greatly influenced by global atmospheric circulation (Li et al., 2020; Sun and Lotz, 2020). Figure.S3d shows that there is a significant correlation between the ENSO index and lake inflow on a 0–5-year scale, highlighting the impact of El Niño events on runoff in Hulun basin. WTC results (Fig.S3e) show that NAO has a strong positive correlation with flow during the 1980s and the 1990s. The strong NAO introduced more precipitation in the basin Siderius et al. (2018), which may be the reason why Hulun Lake maintained high WLs during this period. Overall, results show that large-scale climate patterns can significantly regulate precipitation in the basin and affect the runoff, thereby indirectly affecting the lake WL.

The direct and indirect effects of climatic factors on WL changes during different periods were explored using the SEM. As shown in Fig. 6a, there is a direct pathway between ET_p and WL. Since the increasing trend of ET_p was notably larger than that of Pre and Tmp (Fig. 3), its impact on WL was more significant (r = −0.67) in the past 60 years. Tmp had the greatest impact on ET_p (r = 0.44), indicating that the rise in ET_p caused by climate warming was the main driving force leading to the decline of Hulun Lake WL,

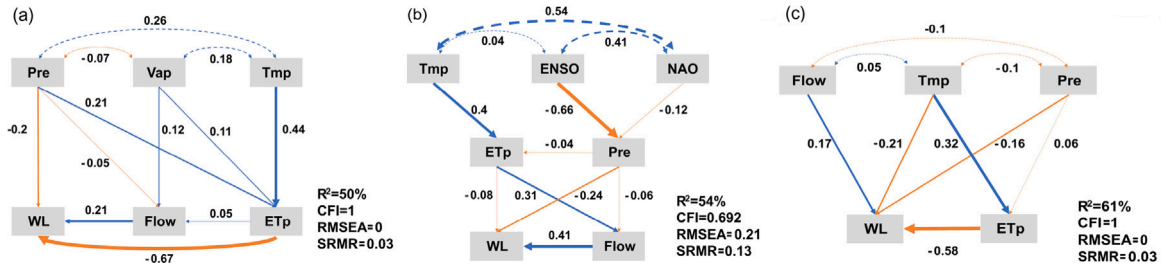

Fig. 6. Results of SEM analysis for (a) 1961–2020, (b) 1961–1997, and (c) 1998–2020. The total coefficient combines the direct and indirect effect of each variable on WL.

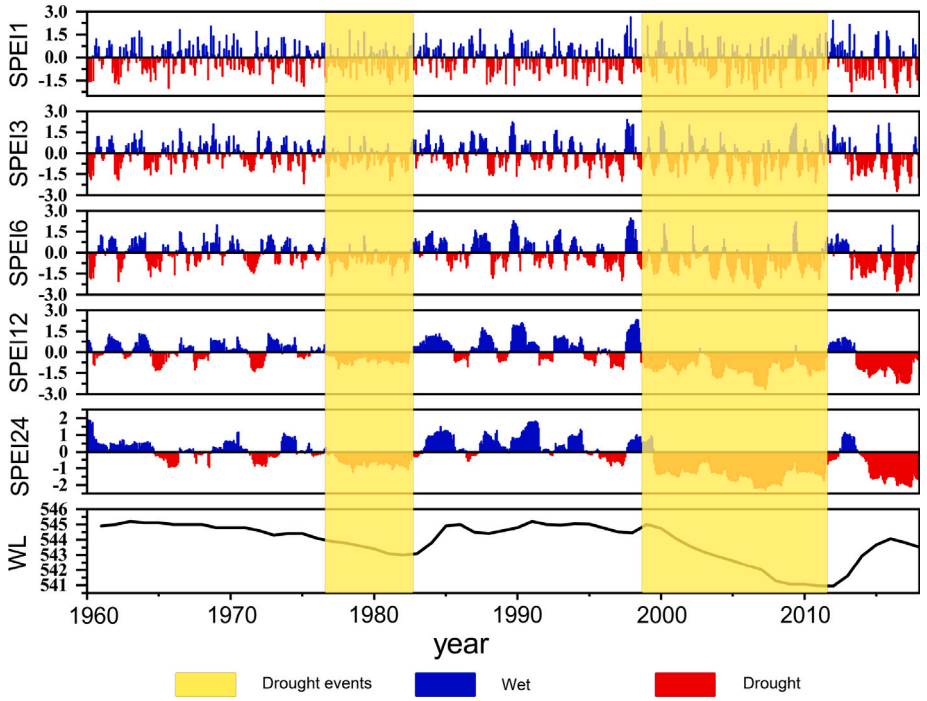

Fig. 7. Time series of SPEI-1, SPEI-3, SPEI-6, SPEI-12 and SPEI-24 for 1961 to 2018.

since it increases lake surface evaporation which plays the largest role of the multi-year water cycle in Hulun Lake (Fu et al., 2021). Moreover, the increasing trend of ET_p was notably larger than that of Pre and Tmp, thus its impact on WL was more significant. Considering both Tmp and ET_p increases may incur drought, the SPEI was used to analyze drought in Hulun Basin. Drought years were often accompanied by a decline in WL, such as in 1977–1983 and 1998–2012 (see Fig. 7). After 2000, The drought became even more severe in terms of intensity and duration. WTC (Fig.S4) showed that long-term drought in the watershed affected the WL throughout the study period. The effect of Pre on Flow is not significant, which is attributed to the high spatial heterogeneity of Hulun Basin. This can cause inconsistent responses of the hydrological cycle to the underlying surface in different regions (Bai et al., 2021), resulting in asynchronous rainfall-runoff-confluence (Zhang et al., 2022). WTC results also verified that there was a time lag between the Flow and Pre (Fig.S5). The total coefficients of ET_p, Pre, Tmp, Flow, and Vap on WL variation were −0.66, −0.3, −0.29, 0.21 and −0.04, respectively.

In the first period, Flow had the greatest impact on WL (r = 0.41; Fig. 6b), indicating that the decrease in runoff (0.1 billion m^3/a) was the main reason for the drop in WL during 1961–1997. The direct effect of ET_p on WL was small (r = −0.08), however, a pathway between ET_p and flow was observed. Due to the existence of a large water-deficient steppe in Hulun Basin Cao et al. (2021b), the increase in ET_p weakens the runoff in the watershed (Chi et al., 2018), indirectly affecting WL by cutting lake inflow (r = −0.24). Previous studies have shown that, although rainfall is an important component of the hydrological cycle in Hulun Basin, runoff is the main source for the water balance of the lake (Haghighi and Klove, 2015). In addition, the strong El Niño greatly enhanced the possibility of summer extreme precipitation (r = −0.66), making the runoff high in the mid-1980s (Fig.S3a) and WL also increased significantly, which is consistent with the increasing trend of extreme precipitation events in Inner Mongolia over the past 50 years (Fu et al., 2013). The effect of NAO on Pre was smaller (r = −0.12) compared to the ENSO. The total coefficients of

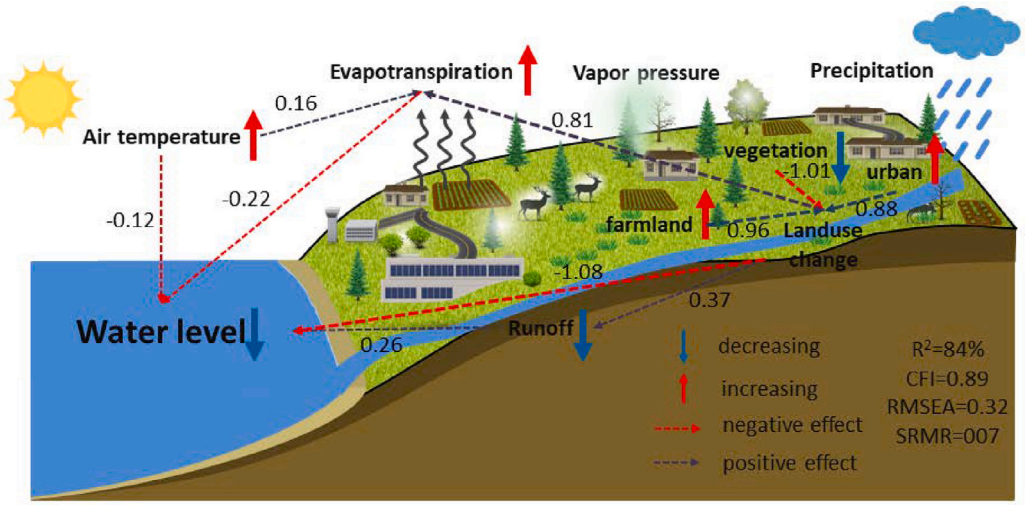

Fig. 8. Mechanism of WL drop during 1998–2020.

Table 2
Correlation analysis between lake levels, flow, and climatic factors in the Hulun Basin during 2011–2017.

	Correlation r	*p*-value
Flow	0.37	0.07
Diversion	0.75	0.05
Vap	−0.22	0.08
Pre	−0.03	0.015
Tmp	0.25	0.17
ET_p	0.29	0.09

Flow, Pre, ENSO, ET_p, Tmp and NAO on WL variation were 0.41, 0.29, −0.19, −0.18, −0.07 and −0.01, respectively. In the second period, ET_p had the greatest impact on WL (r = −0.58; Fig. 6c). The rising temperature was a reason for the increase in ET_p (r = 0.32). In addition, rising Tmp facilitates the decline in WL (r = −0.21). This is because the areas of permafrost in the upper reaches of the Ursun and Kherlen rivers have been decreasing, and the snow melt in mountainous areas has accelerated since the 1980s, which to a certain extent replenished the river flow and maintained high WL. However, around 2000, as Tmp continued to rise, the permafrost layer completely disappeared (Sun and Lotz, 2020), and the insufficient supply of snow-thawed permafrost to the rivers caused lake inflow to decline rapidly. Thus, WL also dropped. The total coefficients of ET_p, Tmp, Pre and Flow on the WL variation were −0.58, −0.4, −0.19, and 0.17, respectively.

4.2. Implication from increased ET_p

In addition to climate change, strong human activities such as deforestation and the expansion of cropland and urbanization are other reasons for the shrinking lake areas in the Mongolia-Xinjiang Plateau after the 1990s (Tao et al., 2015). Cropland increased by 3919 km^2 from 1992 to 2020. The significant expansion of cropland altered the properties of land surface, such as surface albedo and leaf area index (Glenn et al., 2010), thereby greatly increasing ET_p in the central watershed and agricultural areas. Urban areas are also expanding, the construction of urban reservoirs, ponds, and roads will intercept surface runoff, thus reducing the amount of water entering the lake (Shirmohammadi et al., 2020). In addition, large areas of forest and vegetation in the upper reaches were replaced by bare land, weakening the retention ability of soil to conserve water. The sediment content of rivers increased in flood season and discharge decreased significantly in dry season, thus threatening water resources and lake WLs (Acosta-Martinez et al., 2010). The SEM was adjusted in the second period after considering the impact of land use change (Fig. 8). Vegetation coverage loss had the most significant impact on WL (r = 1.09), followed by the expansion of cultivated land and urban areas (r = −1.04, r = −0.95). Land use change had the most significant impact on the increase in ET_p (r = 0.78). The total coefficients of LC, Flow, ET_p and Tmp on WL variation were −0.86, 0.26, 0.2, and 0.02, respectively. Overall, the decline in the WL of Hulun Lake in the late 1990s was the result of the combined effects of climate warming, vegetation degradation, and urban and cropland expansion.

Notably, Hulun Basin experienced severe drought during 2013–2020 (Fig. 7). However, the WL began to rise at a rate of 312 mm/a since 2012. Correlation analysis (Table 2) showed that from 2012 to 2020, the correlation between the inflow and WL was 0.75, exceeding the correlations of natural inflow and meteorological factors with WL. The rapid recovery of the WL can be explained by the implementation of the river diversion project, which was introduced in 2010 (Cai et al., 2016).

From 1961 to 1997, Hulun Basin was less disturbed and the WL was mainly affected by climate change. Reduction in runoff caused the slight WL decrease, which is consistent with the results found by Cao et al. (2021a) and Fu et al. (2021). During this time, the WL generally fluctuated within a certain range; however, the WL underwent drastic changes after 1998. At the beginning of the 21st century, ET_p of the basin increased significantly due to the rising temperature, which is considered to be the main reason for WL drop (Fan et al., 2021). While, in our work, we found that the landuse of Hulun Basin has changed a lot since the late 20st century. As a consequence, vegetation degradation, and human activities further increased the ET_p, resulting in a decrease in the water yield of the basin. The increasing warming and drying trends and drought events in the Hulun Basin have seriously threatened the water yield here, and a reasonable land-use pattern can promote surface runoff yield by conserving water resources, thus ensuring lake inflow (Sun et al., 2017). Forest land can better reduce the fluctuation of water production in the basin caused by climate change (Feng et al., 2012) and protect the regional environment from extreme events (Lloret et al., 2012). In the future, while ensuring ecological water replenishment, the focus should be further strengthened by performing ecological restoration based on forest land and shrubs that are conducive to runoff in order to preserve soil water storage and canopy interception capacity, thus ultimately to improve inflow to maintain a suitable ecological WL for Hulun Lake.

5. Conclusions

This study applied wavelet analysis to explore the characteristics of Hulun Lake WL and the changing climate factors in the basin. Results showed that in the past 60 years, Hulun basin has shown a warming trend, while the WL has shown an overall downward trend (41.2 mm/a), which can be further divided into two periods, namely a slow declining period from 1961 to 1997 where the WL decreased with a trend of 7.4 mm/a, and a transitional period towards recovery from 1998 to 2020 where WL dropped by 3.47 m and began to rise in 2012, with an overall decrease of 37.6 mm/a. Using SEM method, the contribution of climatic factors to WL was quantified and the driving mechanism of WL change was revealed, which showed that the increasing ET_p caused by warming temperature was the main reason for WL decline ($r = -0.66$). From 1961 to 1997, increasing ET_p led to reduced runoff, which directly caused a decrease in WL ($r = 0.41$). In the mid-1980s, the ENSO drove the increasing rainfall and incurred a slight increase in WL (r = 0.31). From 1998 to 2020, land use change became the main reason for the decline in lake WL ($r = -1.08$), because the basin experienced significant deforestation, farmland expansion, and urbanization, which significantly enhanced ET_p ($r = -0.22$) and further reduced runoff, leading to a WL drop. With a mandate of ecological water protection from the government, future efforts should focus on implementing ecological restoration by recovering forests, grasses, and shrubs lands that are conducive to runoff in order to increase lake inflow and maintain a suitable WL.

Still, some limitations of this work should be noted. First, the proposed method does not describe lake level dynamics as physics-based models do, and it cannot capture all nonlinear relationships among possible driving factors and WL. Thus, further studies are still needed to investigate such non-linear relationships. In addition, a longer water diversion data may help to better elaborate the driving mechanism of WL variation.

CRediT authorship contribution statement

Yuqi Huang: Conceptualization, Methodology, Software. **Bo Yao:** Reviewed the manuscript. **Yu Li:** Reviewed the manuscript, Supervised the research. **Hao Zhang:** Writing – original draft. **Shengrui Wang:** Conceptualization, Supervision, Funding.

Declaration of competing interest

The authors declare that they have no known competing financial interests or personal relationships that could have appeared to influence the work reported in this paper.

Data availability

Data will be made available on request.

Acknowledgments

This research was funded by the National Key Research and Development Project of China, grant number (2019YFC0409201), the Guangdong-Hong Kong Joint Laboratory for Water Security, grant number (2020B1212030005) and National High-level Personnel of Special Support Program (People Plan, grant number 312232102). We are very grateful to all the datasets producers.

Appendix A. Supplementary data

Supplementary material related to this article can be found online at https://doi.org/10.1016/j.ejrh.2023.101352.

References

Acosta-Martinez, V., Bell, C.W., Morris, B.E.L., Zak, J., Allen, V.G., 2010. Long-term soil microbial community and enzyme activity responses to an integrated cropping-livestock system in a semi-arid region. Agric. Ecosys. Environ. 137 (3–4), 231–240.

Bai, M., Mo, X., Liu, S., Hu, S., 2021. Detection and attribution of lake water loss in the semi-arid Mongolian Plateau-A case study in the Lake Dalinor. Ecohydrology 14 (1).

Cai, Z., Jin, T., Li, C., Ofterdinger, U., Zhang, S., Ding, A., Li, J., 2016. Is China's fifth-largest inland lake to dry-up? Incorporated hydrological and satellite-based methods for forecasting Hulun lake water levels. Adv. Water Resour. 94, 185–199.

Cao, Y., Fu, C., Wang, X., Dong, L., Yao, S., Xue, B., Wu, H., Wu, H., 2021a. Decoding the dramatic hundred-year water level variations of a typical great lake in semi-arid region of northeastern Asia. Sci. Total Environ. 770.

Cao, Y., Fu, C., Wang, X., Dong, L., Yao, S., Xue, B., Wu, H., Wu, H., 2021b. Decoding the dramatic hundred-year water level variations of a typical great lake in semi-arid region of northeastern Asia. Sci. Total Environ. 770.

Chen, L., Dai, Y., Zhi, X., Xie, H., Shen, Z., 2018. Quantifying nonpoint source emissions and their water quality responses in a complex catchment: A case study of a typical urban-rural mixed catchment. J. Hydrol. 559, 110–121.

Chi, D., Wang, H., Li, X., Liu, H., Li, X., 2018. Estimation of the ecological water requirement for natural vegetation in the Ergune River basin in Northeastern China from 2001 to 2014. Ecol. Indic. 92, 141–150.

Cooley, S.W., Ryan, J.C., Smith, L.C., 2021. Human alteration of global surface water storage variability. Nature 591 (7848), 78–+.

Cretaux, J.F., Jelinski, W., Calmant, S., Kouraev, A., Vuglinski, V., Berge-Nguyen, M., Gennero, M.C., Nino, F., Abarca Del Rio, R., Cazenave, A., Maisongrande, P., 2011. SOLS: A lake database to monitor in the near real time water level and storage variations from remote sensing data. Adv. Space Res. 47 (9), 1497–1507.

Fan, C., Song, C., Liu, K., Ke, L., Xue, B., Chen, T., Fu, C., Cheng, J., 2021. Century-scale reconstruction of water storage changes of the largest lake in the inner Mongolia Plateau using a machine learning approach. Water Resour. Res. 57 (2).

Fang, C., Song, K.S., Shang, Y.X., Ma, J.H., Wen, Z.D., Du, J., 2019. Remote sensing of harmful algal blooms variability for lake Hulun using adjusted FM (AFAI) algorithm. J. Environ. Informat. 34 (2), 108–122.

Feng, X.M., Sun, G., Fu, B.J., Su, C.H., Liu, Y., Lamparski, H., 2012. Regional effects of vegetation restoration on water yield across the Loess Plateau, China. Hydrol. Earth Syst. Sci. 16 (8), 2617–2628.

Fu, C., Wu, H., Zhu, Z., Song, C., Xue, B., Wu, H., Ji, Z., Dong, L., 2021. Exploring the potential factors on the striking water level variation of the two largest semi-arid-region lakes in northeastern Asia. Catena 198.

Fu, G., Yu, J., Yu, X., Ouyang, R., Zhang, Y., Wang, P., Liu, W., Min, L., 2013. Temporal variation of extreme rainfall events in China, 1961–2009. J. Hydrol. 487, 48–59.

Glenn, E.P., Nagler, P.L., Huete, A.R., 2010. Vegetation index methods for estimating evapotranspiration by remote sensing. Surv. Geophys. 31 (6), 531–555.

Grace, J.B., Adler, P.B., Harpole, W.S., Borer, E.T., Seabloom, E.W., 2014. Causal networks clarify productivity-richness interrelations, bivariate plots do not. Funct Ecol 28 (4), 787–798.

Guclu, Y.S., 2018. Multiple sen-innovative trend analyses and partial Mann-Kendall test. J. Hydrol. 566, 685–704.

Haghighi, A.T., Klove, B., 2015. A sensitivity analysis of lake water level response to changes in climate and river regimes. Limnologica 51, 118–130.

Hao, J., Xu, G., Luo, L., Zhang, Z., Yang, H., Li, H., 2020. Quantifying the relative contribution of natural and human factors to vegetation coverage variation in coastal wetlands in China. Catena 188.

Harris, I., Osborn, T.J., Jones, P., Lister, D., 2020. Version 4 of the CRU TS monthly high-resolution gridded multivariate climate dataset. Sci. Data 7 (1).

Henseler, J., Ringle, C.M., Sarstedt, M., 2015. A new criterion for assessing discriminant validity in variance-based structural equation modeling. J. Acad. Marketing Sci. 43 (1), 115–135.

Hollmann, R., Merchant, C.J., Saunders, R., Downy, C., Buchwitz, M., Cazenave, A., Chuvieco, E., Defourny, P., de Leeuw, G., Forsberg, R., Holzer-Popp, T., Paul, F., Sandven, S., Sathyendranath, S., van Roozendael, M., Wagner, W., 2013. The ESA climate change initiative satellite data records for essential climate variables. Bull. Am. Meteorol. Soc. 94 (10), 1541–1552.

Jia, J., Gao, Y., Zhou, F., Shi, K., Johnes, P.J., Dungait, J.A.J., Ma, M., Lu, Y., 2020. Identifying the main drivers of change of phytoplankton community structure and gross primary productivity in a river-lake system. J. Hydrol. 583.

Kraemer, B.M., Seimon, A., Adrian, R., McIntyre, P.B., 2020. Worldwide lake level trends and responses to background climate variation. Hydrol. Earth Syst. Sci. 24 (5), 2593–2608.

Kundu, S., Khare, D., Mondal, A., 2017. Individual and combined impacts of future climate and land use changes on the water balance. Ecol. Eng. 105, 42–57.

Labat, D., 2005. Recent advances in wavelet analyses: Part I. A review of concepts. J. Hydrol. 314 (1–4), 275–288.

Labat, D., Ronchail, J., Guyot, J.L., 2005. Recent advances in wavelet analyses: Part 2 - Amazon, Parana, Orinoco and Congo discharges time scale variability. J. Hydrol. 314 (1–4), 289–311.

Li, J., Bai, X., Jin, Y., Song, F., Chen, Z., Cai, L., Zou, F., Jiang, M., Yun, R., Lv, Z., 2020. Recent intensified runoff variability in the hailar river basin during the past two centuries. J. Hydrometeorol. 21 (10), 2257–2273.

Li, S., Chen, J., Xiang, J., Pan, Y., Huang, Z., Wu, Y., 2019. Water level changes of Hulun lake in inner Mongolia derived from Jason satellite data. J. Vis. Commun. Image Represent. 58, 565–575.

Li, Y., Li, X., Huang, G., Wang, S., Li, D., 2021. Sedimentary organic carbon and nutrient distributions in an endorheic lake in semiarid area of the Mongolian Plateau. J. Environ. Manag. 296.

Li, S., Wang, G., Zhu, C., Lu, J., Ullah, W., Hagan, D.F.T., Kattel, G., Peng, J., 2022. Attribution of global evapotranspiration trends based on the Budyko framework. Hydrol. Earth Syst. Sci. 26 (13), 3691–3707.

Liu, Y., Yue, H., 2017. Estimating the fluctuation of lake Hulun, China, during 1975–2015 from satellite altimetry data. Environ. Monit. Assess. 189 (12).

Lloret, F., Escudero, A., Maria Iriondo, J., Martinez-Vilalta, J., Valladares, F., 2012. Extreme climatic events and vegetation: The role of stabilizing processes. Global Change Biol. 18 (3), 797–805.

McCombs, M.P., Mulligan, R.P., Boegman, L., 2014. Offshore wind farm impacts on surface waves and circulation in Eastern Lake Ontario. Coast. Eng. 93, 32–39.

Rezaei, A., Gurdak, J.J., 2020. Large-scale climate variability controls on climate, vegetation coverage, lake and groundwater storage in the lake urmia watershed using SSA and wavelet analysis. Sci. Total Environ. 724.

Shirmohammadi, B., Malekian, A., Salajegheh, A., Taheri, B., Azarnivand, H., Malek, Z., Verburg, P.H., 2020. Impacts of future climate and land use change on water yield in a semiarid basin in Iran. Land Degradation Dev. 31 (10), 1252–1264.

Siderius, C., Gannon, K.E., Ndiyoi, M., Opere, A., Batisani, N., Olago, D., Pardoe, J., Conway, D., 2018. Hydrological response and complex impact pathways of the 2015/2016 El Nino in Eastern and Southern Africa. Earths Future 6 (1), 2–22.

Song, X., Zhang, C., Su, X., Zhu, L., Wei, Z., Zhao, Y., 2021. Characteristics of humic substance in lake sediments: The case of lakes in northeastern China. J. Hydrol. 603.

Sun, Z., Lotz, T., 2020. Linking meteorological patterns shift to hydrological extremes in a lake watershed across the mid-high latitude transition region. Stoch. Environ. Res. Risk Assess. 34 (8), 1121–1134.

Sun, Z., Lotz, T., Chang, N.-B., 2017. Assessing the long-term effects of land use changes on runoff patterns and food production in a large lake watershed with policy implications. J. Environ. Manag. 204, 92–101.

Tao, S., Fang, J., Zhao, X., Zhao, S., Shen, H., Hu, H., Tang, Z., Wang, Z., Guo, Q., 2015. Rapid loss of lakes on the Mongolian Plateau. Proc. Natl. Acad. Sci. USA 112 (7), 2281–2286.
Wang, D., 2018. A new probability density function for spatial distribution of soil water storage capacity leads to the SCS curve number method. Hydrol. Earth Syst. Sci. 22 (12), 6567–6578.
Woolway, R.I., Kraemer, B.M., Lenters, J.D., Merchant, C.J., O'Reilly, C.M., Sharma, S., 2020. Global lake responses to climate change. Nature Rev. Earth Environ. 1 (8), 388–403.
Woolway, R.I., Merchant, C.J., 2019. Worldwide alteration of lake mixing regimes in response to climate change. Nat. Geosci. 12 (4), 271–+.
Wu, Y., Shi, X., Zhao, S., Lin, T., Ma, J., 2015. Major ion chemistry and influencing factors of three typical lakes in inner Mongolia Plateau. Ecol. Environ. Sci. 24 (7), 1202–1208.
Xiao, J., Chang, Z., Wen, R., Zhai, D., Itoh, S., Lomtatidze, Z., 2009. Holocene weak monsoon intervals indicated by low lake levels at Hulun lake in the monsoonal margin region of northeastern inner Mongolia, China. Holocene 19 (6), 899–908.
Yang, L., Shen, F., Zhang, L., Cai, Y., Yi, F., Zhou, C., 2021. Quantifying influences of natural and anthropogenic factors on vegetation changes using structural equation modeling: A case study in Jiangsu Province, China. J. Clean. Prod. 280.
Yang, K., Yu, Z., Luo, Y., 2020. Analysis on driving factors of lake surface water temperature for major lakes in Yunnan-Guizhou Plateau. Water Res. 184, 116018.
Yang, K., Yu, Z., Luo, Y., Zhou, X., Shang, C., 2019. Spatial-temporal variation of lake surface water temperature and its driving factors in Yunnan-Guizhou Plateau. Water Resour. Res. 55 (6), 4688–4703.
Zhang, J., Duan, L., Liu, T., Chen, Z., Wang, Y., Li, M., Zhou, Y., 2022. Experimental analysis of soil moisture response to rainfall in a typical grassland hillslope under different vegetation treatments. Environ. Res. 213.
Zhang, Y., Liang, W., Liao, Z., Han, Z., Xu, X., Jiao, R., Liu, H., 2019. Effects of climate change on lake area and vegetation cover over the past 55 years in northeast inner Mongolia grassland, China. Theor. Appl. Climatol. 138 (1–2), 13–25.
Zhang, J., Liu, P., Wang, H., Lei, X., Zhou, Y., 2015. A Bayesian model averaging method for the derivation of reservoir operating rules. J. Hydrol. 528, 276–285.
Zhao, C., Liu, C., Dai, X., Liu, T., Duan, Z., Liu, L., Mitrovic, S.M., 2015. Separation of the impacts of climate change and human activity on runoff variations. Hydrol. Sci. J.-J. Des Sci. Hydrologiques 60 (2), 234–246.
Zhou, Y., Dong, J., Xiao, X., Liu, R., Zou, Z., Zhao, G., Ge, Q., 2019. Continuous monitoring of lake dynamics on the Mongolian Plateau using all available landsat imagery and Google earth engine. Sci. Total Environ. 689, 366–380.